fuels

MDPI

Article

Biochar Surface Chemistry Modification by Blending Hardwood, Softwood, and Refuse-Derived Fuel: Insights from XPS, FTIR, and Zeta Potential Analysis

Paul C. Ani [1], Hasan J. Al-Abedi [1], Joseph D. Smith [1,*] and Zeyad Zeitoun [2]

[1] Linda and Bipin Doshi Department of Chemical and Biochemical Engineering, Missouri, University of Science and Technology, Rolla, MO 64501, USA; pcaz3w@mst.edu (P.C.A.); alabedih@mst.edu (H.J.A.-A.)
[2] Department of Engineering and Computer Science, McNeese State University, Lake Charles, LA 70607, USA; zzeitoun@mcneese.edu
* Correspondence: smithjose@mst.edu

Abstract

This study investigates how the inclusion of refuse-derived fuel (RDF) alters the surface chemistry and electrostatic behavior of oak-based biochar. Biochars were produced using downdraft gasification at 850 °C from 100% oak (HW) and a ternary blend comprising 50% oak, 30% pine, and 20% RDF (HW/SW/RDF). Characterization using Fourier transform infrared spectroscopy (FTIR), X-ray photoelectron spectroscopy (XPS), zeta potential, pH, and electrophoretic mobility was conducted to assess surface functionality and colloidal behavior. The RDF-containing biochar exhibited a 43.3% increase in surface nitrogen content (from 0.24% to 0.90%) and a 6.6% rise in calcium content (from 2.07% to 2.27%) alongside the introduction of chlorine (0.20%) and elevated silicon levels (0.69%) compared to RDF-free counterparts. A concurrent reduction in oxygen-containing functional groups was observed, as O1s decreased from 15.75% in HW to 13.37% in HW/SW/RDF. Electrokinetic measurements revealed a notable decrease in zeta potential magnitude from −31.5 mV in HW to −24.2 mV in HW/SW/RDF, indicating diminished surface charge and colloidal stability. Moreover, the pH declined from 10.25 to 7.76, suggesting a loss of alkalinity and buffering capacity. These compositional and electrostatic shifts demonstrate that RDF inclusion significantly modifies the surface reactivity of biochar, influencing its performance in catalysis, ion exchange, and nutrient retention. The findings underscore the need for tailored post-treatment strategies to enhance the functionality of RDF-modified biochars in environmental applications.

Keywords: biochar; surface chemistry; refuse-derived fuel (RDF); oak-based biomass zeta potential; electrophoretic mobility

Academic Editor: Martin Olazar

Received: 11 July 2025
Revised: 25 August 2025
Accepted: 2 September 2025
Published: 22 September 2025

Citation: Ani, P.C.; Al-Abedi, H.J.; Smith, J.D.; Zeitoun, Z. Biochar Surface Chemistry Modification by Blending Hardwood, Softwood, and Refuse-Derived Fuel: Insights from XPS, FTIR, and Zeta Potential Analysis. *Fuels* **2025**, *6*, 71. https://doi.org/10.3390/fuels6030071

1. Introduction

Biochar continues to gain prominence in environmental technology due to its unique surface chemistry and potential for carbon stabilization, contaminant adsorption, and soil pH modulation. The efficacy of biochar in these applications is largely governed by its surface functionality, including the abundance of oxygen-containing groups, mineral interactions, and electrostatic properties. These characteristics are, in turn, highly dependent on both the feedstock composition and the thermochemical conversion process employed [1,2].

Among the various production methods, downdraft gasification provides a consistent and scalable route to generate biochar under high-temperature conditions, typically above

800 °C. Biochar produced at such elevated temperatures tends to exhibit lower volatile content, higher carbon purity, and more ordered carbon structures [3–7]. However, while high-temperature gasification improves thermal properties, it also significantly affects the chemical functionality on the biochar surface, often leading to a reduction in polar and acidic groups that are vital for ion exchange and adsorption processes [5,8].

Feedstock selection plays a central role in determining the chemical nature of biochar surfaces. Oak, a hardwood with a dense lignocellulosic structure, is commonly used for its ability to yield structurally stable and chemically consistent biochar [9]. In recent years, there has been increasing interest in integrating non-traditional materials such as refuse-derived fuel (RDF) into the gasification process [10,11]. RDF consists of various processed municipal waste components and introduces a heterogeneous mixture of organics, inorganics, and synthetic materials. When combined with wood biomass in gasification, RDF has been shown to alter the elemental and ash composition of the resulting char. However, its impact on surface chemistry and electrostatic behavior, particularly when gasified at high temperatures in a downdraft reactor, remains poorly understood [12–14].

Biomass-derived graphene quantum dots (GQDs) produced using green hydrothermal methods have shown that organic waste can yield uniform nanoscale materials with high optical performance. These GQDs, rich in oxygen- and nitrogen-based surface groups, combine stability with enhanced reactivity, underscoring the value of waste-derived carbon nanomaterials for catalytic, sensing, and remediation uses—aligning closely with the objectives of RDF-modified biochar [15].

The novelty of this study lies in its focused investigation of RDF-modified biochar surface properties through a rigorous combination of XPS, FTIR, zeta potential, and pH-based surface charge analysis. While earlier studies have acknowledged the compositional effects of RDF, yield, and energy composition, few have explored in depth how RDF-induced chemical variability directly influences surface charge dynamics, functional group abundance, and electrostatic buffering behavior. This study uniquely quantifies RDF's influence at both the molecular and electrochemical levels, highlighting its significance in tailoring biochar for targeted environmental applications [4,16].

This study addresses this gap by examining the surface chemical and electrosurface properties of biochar produced from 100% oak (HW); a blend of oak and pine in a 1:1 ratio; and a blend of 50% oak, 30% pine, and 20% RDF. All the samples were generated using a downdraft gasifier operated at 850 °C to ensure consistent thermal history. The study focuses on characterizing surface functional groups using Fourier transform infrared spectroscopy (FTIR), identifying elemental surface composition via X-ray photoelectron spectroscopy (XPS), and evaluating surface charge behavior through zeta potential measurements, pH analysis, and electrophoretic mobility [17].

To achieve a detailed understanding of these transformations, the study leverages complementary characterization tools: XPS for surface elemental profiling and oxidation state identification, FTIR for functional group analysis, zeta potential for assessing electrostatic stability and colloidal dispersion, and pH measurements to evaluate surface alkalinity and buffering behavior. These techniques collectively provide mechanistic insight into how RDF alters the surface chemistry interface of biochar, enabling more informed decisions on its environmental deployment [18–20].

The objective is to determine how RDF inclusion alters surface acid-base characteristics, charge potential, and chemical composition at the micro-scale. Such properties are critical for evaluating the suitability of biochar in environmental applications where ion exchange, contaminant adsorption, or colloidal stability play a significant role. By isolating RDF's influence on surface reactivity, this study provides insight into how waste-derived

feedstocks affect the interfacial behavior of biochar and informs future efforts in tailoring biochar for specific environmental functions [1,21,22].

Furthermore, this work responds to existing research gaps by explicitly addressing the variability of RDF composition—a factor often overlooked in prior studies. Municipal RDF streams vary in plastic, organic, and inorganic content, which in turn impacts the reproducibility and performance of RDF-amended biochar. This study examines how such variability affects elemental enrichment (e.g., N, Ca, Cl, Si), functional group distribution, and overall surface reactivity, thereby shedding light on the complex interplay between RDF heterogeneity and biochar functionality [23,24].

Past investigations have explored RDF addition at various levels, yet few have systematically correlated RDF proportion with zeta potential, functional group shifts, and changes in electrochemical stability. This work fills that void by offering a detailed physicochemical mapping of RDF effects in a controlled 20% RDF blend—a proportion representative of real-world scenarios—while setting the stage for future studies involving graded RDF additions and post-treatment enhancements [12].

2. Materials and Methodology

The biochar samples investigated in this study were prepared from selected biomass feedstocks using a downdraft gasifier operated at a controlled temperature of 850 °C. The study made use of three different types of feedstocks: pure oak pellets, an equal blend of oak and pine pellets, and a third mixture containing 50% oak, 30% pine, and 20% refuse-derived fuel (RDF) by weight.

2.1. Biochar Preparation

The oak and pine pellets were commercially obtained from Lowe's Home Improvement store in Rolla, Missouri, USA. The refuse-derived fuel (RDF), made up of pre-processed combustible materials from municipal waste, was supplied by Idaho National Laboratory, USA. These pellets were introduced into a laboratory-scale downdraft gasifier equipped to operate under controlled temperature conditions, with the combustion zone maintained at an average of 850 °C. The downdraft reactor design facilitated sequential stages of drying, pyrolysis, oxidation, and reduction, with a residence time of 45–60 min, producing stable, high-carbon biochar. Air was supplied as the gasifying agent through an induced draft mechanism, with the superficial velocity regulated to optimize reaction kinetics and enhance tar reduction. Figure 1 presents a laboratory-scale gasifier with a one-ton-per-day capacity of biochar via downdraft gasification. The gasification process and system configuration have been extensively discussed in prior work and are referenced herein for methodological details [25].

Images of feedstock pellets and produced biochar are presented in Figure 2 to illustrate their physical appearance following gasification.

2.2. Surface and Electrochemical Characterization

To evaluate the surface chemistry and electrostatic behavior of the produced biochar samples, a combination of Fourier transform infrared spectroscopy (FTIR), X-ray photoelectron spectroscopy (XPS), and electrochemical analyses—including zeta potential, conductivity, and electrophoretic mobility—was employed. All measurements were conducted in triplicate to ensure reproducibility.

2.2.1. X-Ray Photoelectron Spectroscopy (XPS)

XPS measurements were carried out using a Thermo Scientific Nexsa system (East Grinstead, UK), featuring a monochromatic Al Kα source and equipped with charge neutralization and angle-resolved analysis capabilities. Surface chemical states and elemental

composition were evaluated following ISO 18115-1. All spectra were analyzed using Advantage software (version 6.8.0). This allowed the quantification of functional groups on the biochar surface, which are crucial for understanding the alteration in surface chemistry due to RDF incorporation [26].

Figure 1. Downdraft gasifier.

Figure 2. Images of gasified biochar (**A**), RDF (**B**), pine (**C**), and oak (**D**).

2.2.2. FTIR Spectroscopy

FTIR analysis was performed to identify surface functional groups using a Thermo Scientific Nicolet iS10 FTIR spectrometer (Madison, WI, USA) operating in transmission mode. Biochar samples were finely ground, mixed with potassium bromide (KBr), and pressed into translucent pellets. Spectra were recorded across a wavenumber range of 4000–400 cm^{-1} with a resolution of 4 cm^{-1}. The FTIR spectral data provided insight into the evolution of oxygenated and aromatic surface groups due to RDF inclusion. Detailed analytical procedures and absorption band interpretations are also referenced from previously published work [25].

2.2.3. pH Measurement

Biochar pH was measured using a calibrated Mettler Toledo instrument in a 1:10 biochar-to-deionized water ratio. Samples were ground and allowed to equilibrate before measurement.

2.2.4. Zeta Potential and Electrophoretic Mobility

Electrophoretic mobility, zeta potential, and electrical conductivity were measured using the Lite Sizer 500 (Anton Paar), following ISO 13099-2 and ISO 7888 standards [27,28]. The samples were ground and suspended in deionized water (1:10 ratio) and ultrasonicated for 60 min to ensure uniform dispersion. Additionally, to investigate the influence of pH on electrostatic surface behavior, a Metrohm 867 pH module was connected in tandem with the LiteSizer 500. This integrated setup enabled real-time pH versus zeta potential correlation, allowing for enhanced interpretation of colloidal behavior as a function of surface charge variation across different pH levels. This approach provided further insight into the impact of RDF inclusion on charge modulation and electrokinetic stability under varying environmental conditions. This analysis enabled the evaluation of colloidal stability and potential environmental interactions.

Further procedural specifics, including instrumentation, techniques, and reproducibility protocols, are documented in the previously published study and are referred to for continuity and methodological transparency [25].

3. Results and Discussion

This section presents a detailed comparison of the surface characteristics and electrochemical behavior of three biochar samples produced using hardwood (HW), a hardwood/softwood blend (HW/SW), and a hardwood/softwood/refuse-derived fuel blend (HW/SW/RDF). The assessment is grounded in X-ray photoelectron spectroscopy (XPS), Fourier transform infrared spectroscopy (FTIR), and zeta potential analysis to explore how the inclusion of RDF influences elemental surface composition, functional groups, and electrostatic properties relevant to catalysis and nutrient exchange processes.

3.1. Surface Elemental Composition and Chemical State Analysis Using XPS

X-ray photoelectron spectroscopy (XPS) was employed to assess the surface elemental composition and chemical states of the three biochar samples derived from oak (HW), oak–pine blend (HW/SW), and a ternary blend including refuse-derived fuel (HW/SW/RDF) [29]. The surface analysis revealed subtle but meaningful compositional changes that reflect the influence of RDF inclusion on the biochar's surface chemistry and potential environmental interactions [30]. Figure 3 presents the graphical results of the XPS survey spectrum for analysis and discussion of the three (3) biochar samples.

Across all samples, carbon (C1s) dominated the surface composition, as expected in carbonaceous materials. The C1s content showed a slight increase from 81.08% in HW to 82.45% in HW/SW and 82.58% in HW/SW/RDF. This trend suggests that the integration of softwood and RDF into the feedstock may support marginally improved carbon retention during gasification, likely influenced by differences in lignocellulosic content and pyrolytic behavior [31].

The oxygen content (O1s) was highest in the oak-derived sample (15.75%) and decreased in the oak–pine blend (13.02%). However, the RDF-containing sample (HW/SW/RDF) registered a slight increase to 13.37%, likely attributable to oxygen-rich constituents within the RDF, such as oxidized polymers or moisture-laden organic waste. These variations imply that oxygen-containing functional groups were more prevalent in the oak biochar, while RDF inclusion introduced secondary oxygenated species that contributed to overall surface oxidation [25].

A more pronounced change was observed in the nitrogen (N1s) content. HW showed a minimal nitrogen presence (0.16%), which increased in HW/SW (0.24%) and rose sharply to 0.90% in HW/SW/RDF. The surge in nitrogen content in the RDF blend points to the introduction of nitrogen-bearing compounds from materials such as food residues

or synthetic waste, potentially enhancing the biochar's capacity for nutrient exchange or catalytic applications [32].

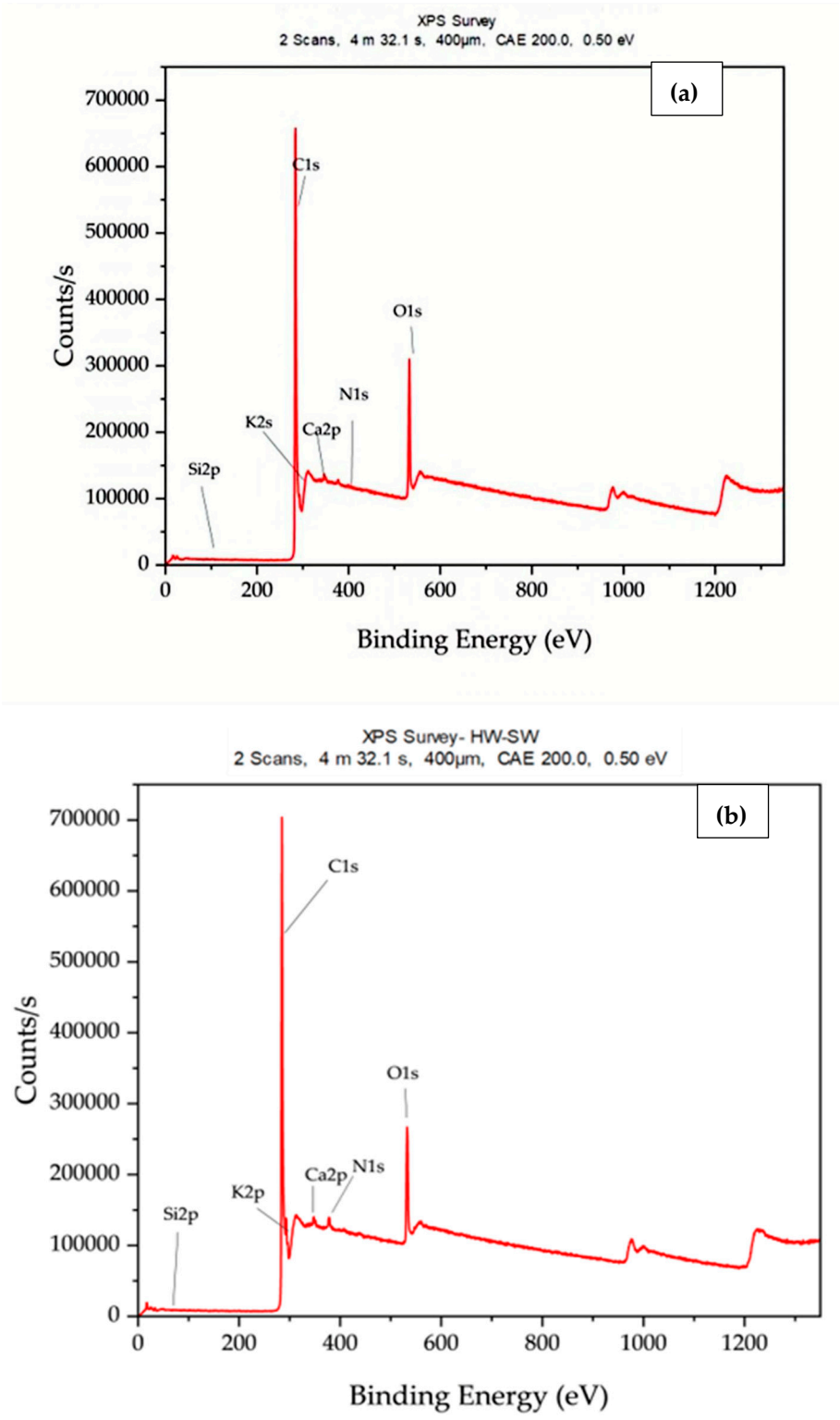

Figure 3. *Cont.*

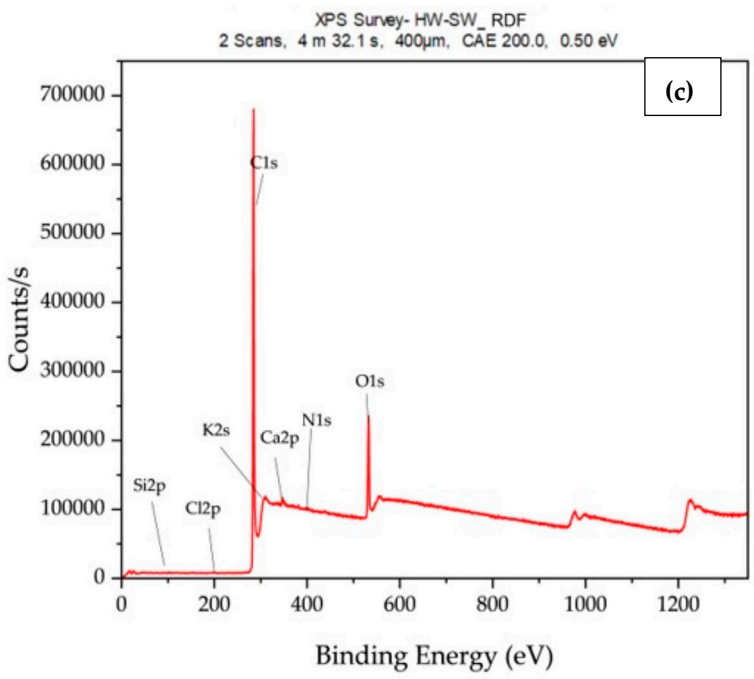

Figure 3. Graph of XPS survey spectrum—HW (**a**), HW/SW (**b**), and HW/SW/RDF (**c**).

Calcium (Ca2p) content followed a similar upward trend, increasing from 1.22% in HW to 2.07% in HW/SW and 2.27% in HW/SW/RDF. This progressive enrichment likely stems from the presence of calcium-based additives or mineral content inherent in the RDF material. The calcium detected appears predominantly in the form of calcium carbonate ($CaCO_3$), as indicated by its binding energy, rather than calcium oxide (CaO) [33,34]. Calcium may enhance the biochar's buffering capacity and heavy metal immobilization potential, although excessive concentrations could impact soil nutrient balances [35,36].

Silicon (Si2p) presented notable variability. While the HW sample contained 0.37%, this dropped to 0.11% in the HW/SW blend, then rose sharply to 0.69% in the HW/SW/RDF sample. This increase is consistent with the introduction of silica-rich debris, such as glass fragments or mineral fillers, commonly found in RDF streams. These inclusions can contribute to structural rigidity but may reduce surface reactivity if not adequately integrated into the biochar matrix [11].

Potassium (K2p) was present in HW (1.41%) and increased in HW/SW (2.11%) but was undetected in the RDF-containing sample. The absence in HW/SW/RDF could result from the formation of potassium chloride (KCl) through interactions between potassium and RDF-derived chlorine during gasification. Given the high temperatures of the process, KCl is likely volatilized and lost from the solid phase. Potassium plays an important role in soil fertility, and its absence may diminish the agronomic value of RDF-amended biochar [37,38].

Chlorine (Cl2p) appeared exclusively in the HW/SW/RDF sample (0.20%), reflecting its origin in plastic materials or chlorinated waste streams. While low in concentration, chlorine's presence could influence the biochar's chemical behavior, posing implications and operational risks, including the potential for dioxin and furan formation during high-temperature processing as well as an increase in soil salinity and potential leachate toxicity in certain applications [39–41].

Finally, these findings reinforce the role of RDF as a modifier of surface chemistry in carbonaceous materials. The inclusion of RDF introduces both beneficial and limiting elements—enriching the biochar with functional heteroatoms like nitrogen and calcium, while also incorporating undesirable components such as chlorine—leading to a possi-

ble depletion of potassium or residual silicon. These chemical changes are critical when considering the biochar's suitability for catalytic applications or soil amendment purposes, especially where ionic exchange capacity, metal sorption, or electrostatic behavior is essential [42,43].

Overall, the XPS results confirm that RDF inclusion significantly alters the surface characteristics of oak-based biochar. While offering the potential for resource recovery and material functionalization, these modifications also demand careful evaluation of environmental safety and compatibility.

The relevance and reliability of XPS in this context are further supported by previous studies. For instance, Nzediegwu et al. [29] utilized XPS to systematically assess the surface characteristics of various biochars, demonstrating the method's robustness in quantifying elemental composition, oxidation states, and functional groups. Such analytical precision is indispensable for elucidating the physicochemical properties that govern biochar's environmental behavior and functional performance. Table 1 shows a summary of the elemental composition and its constituent weight percentage.

Table 1. Summary of the elemental composition of the three biochar samples.

Element	HW Weight %	HW/SW Weight %	HW/SW/RDF Weight %
N1s	0.164481	0.240593	0.903234
C1s	81.07511	82.45155	82.57513
O1s	15.7526	13.02327	13.36913
Ca2p	1.224915	2.067382	2.271619
Si2p	0.374155	0.109751	0.685372
K2p	1.408742	2.107454	-
Cl2p	-	-	0.195517

3.2. Functional Group Characterization Using FTIR Spectroscopy

Fourier transform infrared (FTIR) spectroscopy was employed to characterize the surface functional groups of the three studied biochar samples [44,45]. The spectral data revealed clear variations in surface chemistry influenced by feedstock composition, particularly the inclusion of RDF, and provided important insights into the material's reactivity, hydrophilicity, and potential electrostatic behavior in environmental applications [44]. Figure 4 presents the FTIR spectrum of the three biochar samples for analysis and discussion.

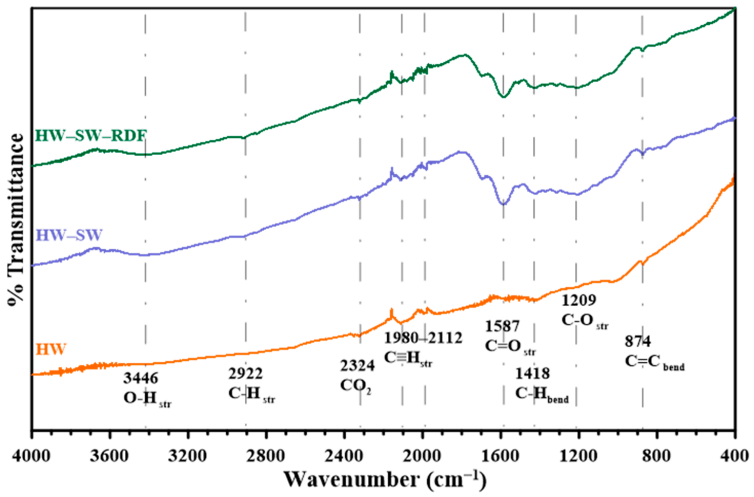

Figure 4. FTIR Spectrum of the three biochar samples.

The (HW) biochar sample showed distinct vibrational peaks indicative of well-defined aromatic and heteroatom-bearing structures. A prominent absorption band at 874 cm^{-1}, located in the fingerprint region, was attributed to aromatic C-H out-of-plane bending, a typical feature of condensed aromatic domains formed during high-temperature gasification [46,47]. The presence of such stable aromatic structures contributes to the structural resilience of the material and supports its persistence in environmental matrices. Additional peaks appearing between 1980 and 2112 cm^{-1} were assigned to nitrile (C≡N) or alkyne (C≡C) groups, suggesting a level of unsaturation and chemical complexity conducive to redox activity or catalytic potential [47–49]. The observed peak at 2200 cm^{-1} may correspond to cumulated double bonds or isocyanate groups (N=C=O), further contributing to the reactivity of the surface [50]. A notable feature at 2324 cm^{-1} likely indicates adsorbed CO_2, a residual product of gasification, potentially retained in the porous structure of the material [51]. These findings reflect a complex array of oxygen- and carbon-based functional groups that enable HW biochar to participate in electrostatic and adsorptive interactions, with relevance to soil remediation and contaminant binding [52,53].

The FTIR profile of the HW/SW sample retained many of the spectral features observed in HW, with some shifts in intensity and additional signals suggesting changes in chemical composition due to the inclusion of softwood. The aromatic C-H peak at 874 cm^{-1} remained prominent, reinforcing the role of lignin-rich structures in maintaining aromaticity. Peaks at 1400, 1500, and 1600 cm^{-1} were attributed to bending vibrations of C-H and C-O bonds, as well as C=C stretching in aromatic systems, indicating a chemically active surface with oxygenated functionalities [54,55]. Peaks at 1587 and 1700 cm^{-1} were linked to conjugated carbonyl groups (C=O), which are often associated with carboxylic acids or aldehydes, adding to the material's polarity and interaction potential with cationic species and chemical activities [46]. Triple bond region peaks (1980–2112 cm^{-1}) again pointed to nitrile or alkyne functionalities, with additional features near 2200 cm^{-1} reinforcing the presence of cumulated systems or isocyanates [50]. The hydroxyl group peak at 3700 cm^{-1} indicated O-H stretching vibrations, likely from alcohol or phenolic groups, enhancing the hydrophilicity of the surface. The surface chemistry of the HW/SW biochar thus reflects a diverse range of functional moieties capable of participating in ion exchange and hydrogen bonding, making it suitable for environmental applications requiring reactive and hydrophilic interfaces [46,56,57].

In the HW/SW/RDF sample, similar functional groups were observed, but with notable differences that reflect the chemical heterogeneity introduced by RDF. While aromatic C-H vibrations persisted at 874 cm^{-1}, other fingerprint region peaks (1400–1600 cm^{-1}) were less pronounced, suggesting possible dilution or disruption of aromatic ordering due to RDF-derived inputs. Stronger or additional bands at 1587 and 1700 cm^{-1} indicated persistent carbonyl groups, which could arise from oxidized RDF constituents such as synthetic polymers or food waste. The triple bond region again featured peaks between 1980 and 2112 cm^{-1} and near 2200 cm^{-1}, indicative of unsaturated and isocyanate groups [50]. A marked signal at 2324 cm^{-1} confirmed the presence of adsorbed carbon dioxide, likely a residual effect of incomplete combustion or retention in micro-pores [51]. The broad O-H stretching band at 3700 cm^{-1} reinforced the surface's hydrophilic nature, though this was likely counterbalanced by structural inconsistencies introduced by RDF [55,58].

Collectively, FTIR spectroscopy has shown that the addition of RDF alters the biochar's surface chemistry without fully compromising key functional groups needed for reactivity. While the HW and HW/SW samples possess balanced compositions favorable for catalysis and sorption, the HW/SW/RDF biochar, although chemically active, may require further structural enhancement—such as activation treatments—to reach comparable efficacy [59].

3.3. Electrostatic Surface Behavior and Colloidal Stability Assessments Using Zeta Potential and Electrophoretic Mobility

The surface charge properties of biochar samples, as revealed by zeta potential and electrophoretic mobility measurements, provide critical insights into their electrostatic stability and interaction behavior in aqueous systems. The zeta potential and electrophoretic mobility of biochar are key indicators of its colloidal stability and surface charge behavior in aqueous systems [27]. These properties influence not only dispersion and colloidal behavior but also the effectiveness of biochar in contaminant binding and nutrient retention across environmental and engineering applications [60]. Figure 5 shows the mean zeta potential distribution curve of the three biochar samples.

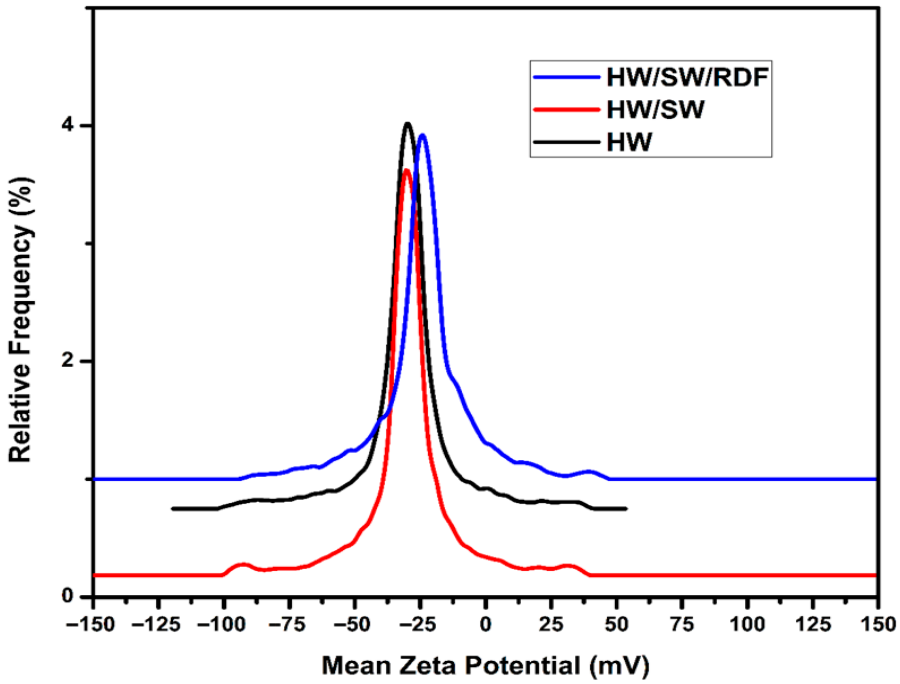

Figure 5. Graph of zeta potential distribution curve for the three biochar samples.

The HW demonstrated the highest magnitude of negative surface charge, with a zeta potential of –31.5 mV. This strong negative value indicates a strong dispersion stability, a surface rich in anionic functional groups, likely carboxylates and phenolic hydroxyls, which contribute to electrostatic repulsion and enhance colloidal stability in suspension. The result suggests a highly stable surface interface in aqueous environments, making this material well-suited for applications in water treatment and contaminant adsorption where uniform dispersion is advantageous [61,62].

In the HW/SW biochar sample, the zeta potential decreased slightly to –30.0 mV. This reduction, though modest, implies a minor attenuation of surface charge density, potentially due to the lower aromatic and polar oxygen-containing group content associated with pine-derived char. Nonetheless, the surface still maintains sufficient negativity to support stability in aqueous phases.

A more pronounced shift was observed in the ternary mixture containing RDF (HW/SW/RDF), where the zeta potential dropped significantly to –24.2 mV. This reduction in surface charge can be linked to the chemical heterogeneity introduced by RDF constituents. The isoelectric point of this sample appears to shift upward, diminishing its net surface charge at neutral pH and weakening its electrostatic repulsion in water. Such a shift implies a less stable dispersion and a greater tendency toward aggregation or sedimentation under environmental conditions.

Correlating these electrokinetic findings with XPS and FTIR data reveals that the decline in zeta potential magnitude is strongly associated with a reduction in oxygen-rich functional groups, particularly carboxylates (–COO^-) and phenolic hydroxyls (–OH). XPS O1s data show a decrease from 15.75% in HW to 13.37% in HW/SW/RDF, indicating a net loss of polar oxygen species. FTIR spectra corroborate this, with diminished intensities in bands attributed to C=O stretching of carboxylic acids (~1700 cm^{-1}) and O–H stretching (~3700 cm^{-1}). These groups contribute negative charges through deprotonation in aqueous environments; their reduction directly limits the development of a strong electrical double layer, explaining the measured shift from −31.5 mV to −24.2 mV [63,64].

The decline in zeta potential magnitude across the three samples reflects the compositional influence of feedstock blending, especially the inclusion of RDF, which appears to disrupt the formation or retention of surface functional groups responsible for negative charge generation. This trend underscores a critical limitation. Specifically, while RDF may contribute to material circularity and waste valorization, it alters the electrostatic behavior of the resulting biochar, reducing its stability and potentially narrowing its applicability in suspension-based systems [12,65].

From a practical standpoint, the loss of a strong negative surface charge and the associated reduction in colloidal stability can impact multiple environmental and catalytic functions. In water remediation, a weaker electrostatic repulsion could reduce the biochar's capacity to adsorb positively charged contaminants such as heavy metal cations or ammonium ions, as these interactions often depend on a highly negative zeta potential [66,67]. In soil systems, reduced charge density may limit cation exchange capacity and slow nutrient cycling [66]. For catalytic uses—such as in advanced oxidation or reduction processes—the diminished presence of electron-donating oxygen functionalities may hinder active site availability and lower reaction rates. These observations suggest that RDF-modified biochar, while chemically enriched in certain heteroatoms, may require post-treatments (e.g., oxidative activation or acid washing) to restore surface polarity and electrostatic performance before deployment in high-performance environmental or catalytic applications [68].

These findings are particularly relevant in contexts where biochar is used in dynamic or fluid environments, such as contaminant transport systems or as a sorbent in water remediation. The results suggest that while oak-based biochar alone or in combination with pine retains desirable electrostatic properties for dispersion and interaction [52], RDF inclusion compromises this advantage. Future studies may explore surface modification techniques or post-treatment strategies to restore or enhance electrostatic stability in RDF-containing biochar [69,70]. Table 2 presents a summary of the disparities in the surface charge of the biochar samples.

Table 2. Summary of the surface charge results of the biochar samples.

Sample	Mean Zeta Potential (mV)	Electrophoretic Mobility (μm.cm/V·s)	pH	Electrochemical Conductivity (μs/cm)
HW	−31.5 ± 0.53	−2.4567	10.10	113 ± 0.123
HW/SW	−30.0 ± 0.64	−2.3385	10.25	170 ± 0.115
HW/SW/RDF	−24.2 ± 0.92	−1.8875	7.76	53 ± 0.172

Further analysis from Table 2 shows that the electrophoretic mobility of the biochar samples exhibited a decreasing trend with feedstock modification. The hardwood biochar (HW) recorded the highest mobility at −2.4567 μm·cm/V·s, reflecting a strongly charged surface capable of stable dispersion. A slight reduction was observed in the HW/SW sample (−2.3385 μm·cm/V·s), suggesting modest attenuation of surface charge density with softwood inclusion. The HW/SW/RDF blend displayed the lowest mobility

(−1.8875 µm·cm/V·s), indicating diminished electrostatic repulsion and a greater propensity for particle aggregation in aqueous systems [71].

Electrochemical conductivity followed a similar pattern. HW and HW/SW samples showed elevated conductivity values of 113 µS/cm and 170 µS/cm, respectively, which may be attributed to the presence of mineral ash species such as potassium and calcium that facilitate ionic movement. Conversely, the HW/SW/RDF sample exhibited a marked decrease in conductivity (53 µS/cm), likely due to dilution of ionizable components and absence of potassium, a strong ionic constituent. These reductions in both mobility and conductivity underscore the influence of RDF on surface charge behavior and ionic interaction potential, which are critical parameters in assessing biochar suitability for environmental and electrochemical applications [72,73].

3.4. Influence of RDF Inclusion on Biochar Alkalinity and Surface pH Characteristics

To better understand the interplay between surface charge and acidity, a pH–zeta potential correlation was conducted by coupling the LiteSizer 500 (Anton Paar) with a Metrohm 867 pH module. This integration enabled real-time tracking of zeta potential as a function of pH, offering a refined perspective on how RDF-induced changes affect the electrostatic profile of the biochar. As shown in Figure 6, a progressive decline in surface charge magnitude with decreasing pH was observed, with the HW/SW/RDF sample displaying the steepest slope. This indicates a reduced buffering capacity and a diminished ability to maintain stable surface charges across a range of pH values.

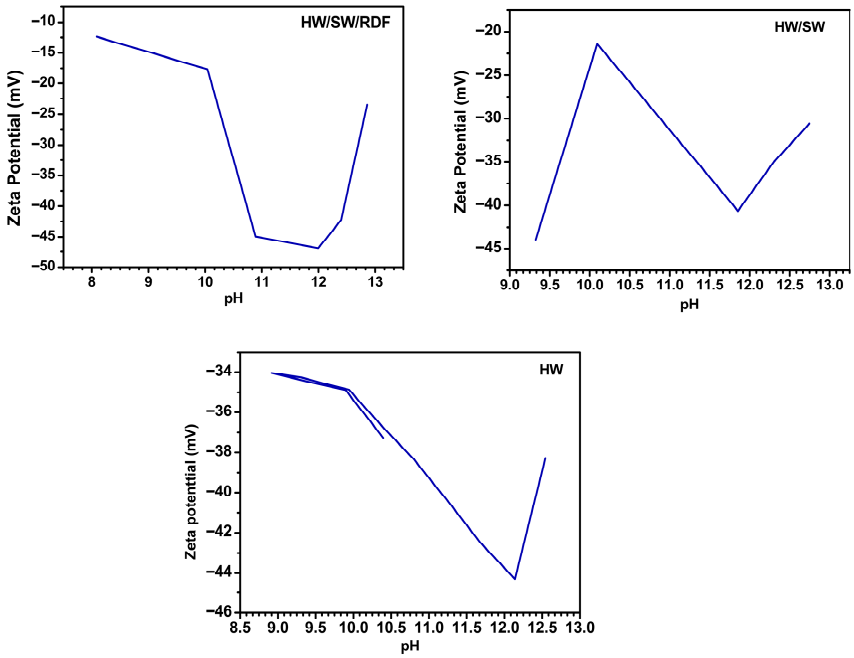

Figure 6. A graph of pH vs. zeta potential for the three samples.

The observed shifts in the pH–zeta potential curve underscore the effect of RDF on colloidal behavior. While HW and HW/SW samples maintained relatively strong negative charges over a broader pH spectrum—supporting robust electrostatic repulsion and colloidal stability—the RDF-containing biochar demonstrated greater sensitivity to pH fluctuations, which could predispose it to aggregation or precipitation in environmental systems. Table 3 presents the comparison table for the three samples and how they changed with pH change [74,75].

Table 3. Comparison of the change of zeta potential with pH for the samples.

Biochar Sample	pH Range	Initial Zeta Potential (mV)	Final Zeta Potential (mV)
HW	9–13	−34	−38
HW/SW	9–13	−44	−30
HW/SW/RDF	8–13	−12.5	−23

Finally, while oak and pine maintain a robust alkaline profile and stability conducive to multiple environmental and catalytic uses, the addition of RDF modifies these properties significantly.

4. Conclusions

This study highlights the significant impact of refuse-derived fuel (RDF) inclusion on the surface chemistry and electrostatic behavior of oak-based biochar. Through detailed XPS, FTIR, and zeta potential analyses, it was evident that RDF-modified biochar exhibits altered elemental composition, reduced oxygen functionalities, and a decline in surface charge stability. These changes were accompanied by a lowered pH and shifts in electrophoretic mobility, suggesting a fundamental transformation of the material's physicochemical interface.

The RDF-containing biochar showed increased surface nitrogen and calcium levels, as well as the introduction of chlorine and silicon, which may influence its suitability for environmental applications. From a catalytic perspective, the rise in heteroatoms such as nitrogen and calcium may enhance surface reactivity and redox potential. Conversely, the observed reduction in oxygen-containing groups and diminished negative zeta potential may hinder interactions reliant on electrostatic attraction, such as metal ion sorption or colloidal stabilization.

Potential drawbacks of RDF inclusion, such as chlorine's presence (0.20%) and associated risks (e.g., dioxin formation, soil salinity), must also be considered to provide a balanced perspective.

In practical terms, these findings have direct implications for industries evaluating RDF-containing biochar systems. Beyond environmental performance, incorporating RDF into biochar production can influence cost–benefit outcomes by valorizing municipal waste streams and potentially reducing feedstock costs. However, trade-offs such as reduced electrostatic stability and the introduction of persistent elements must be weighed, particularly where product consistency is essential for large-scale commercialization. Additionally, RDF-modified biochar presents potential in emerging applications, including the synthesis of advanced nanomaterials.

Looking ahead, future research should focus on tailoring RDF-containing biochar for advanced applications through targeted post-treatments, such as surface activation, acid/base washing for chlorine removal, ammonia activation to enhance nitrogen functionalities, or impregnation with catalytic metals. Such modifications could enhance its catalytic performance in reactions like advanced oxidation processes or improve its ion-exchange capacity for nutrient recovery in agricultural systems. Furthermore, investigating the long-term stability gap will require controlled leaching experiments and aging studies in both soil and aqueous environments to assess persistence, transformation, and safety. Environmental interactions of RDF-modified biochars in soil or aqueous environments will be crucial to fully utilize their potential in circular bioeconomy and waste valorization strategies.

This study advances the current state of knowledge by quantitatively linking RDF-specific chemical signatures—such as elevated nitrogen and calcium levels, alongside

chlorine introduction—to measurable shifts in zeta potential, oxygen functional group abundance, and pH buffering capacity. These correlations distinguish RDF-modified biochar from other modification approaches in the literature. Finally, situating these findings within a circular economy framework underscores the opportunities and responsibilities associated with RDF valorization, including the need to manage emissions of hazardous compounds and persistent inorganics during processing through informed feedstock selection, emission controls, and tailored post-treatments.

Author Contributions: Conceptualization, J.D.S., P.C.A., H.J.A.-A.; methodology, J.D.S., H.J.A.-A.; formal analysis, P.C.A.; investigation, P.C.A. and H.J.A.-A.; resources, J.D.S., H.J.A.-A.; data curation, H.J.A.-A., P.C.A.; writing—original draft preparation, P.C.A., J.D.S., H.J.A.-A., Z.Z.; writing—review and editing, P.C.A., J.D.S., H.J.A.-A., Z.Z.; supervision, J.D.S.; project administration, J.D.S.; funding acquisition, J.D.S. All authors have read and agreed to the published version of the manuscript.

Funding: This research was funded by Syntech Graphene Technologies, LLC.

Conflicts of Interest: The Authors declare no conflict of interest.

References

1. Rajput, V.; Saini, I.; Parmar, S.; Pundir, V.; Kumar, V.; Kumar, V.; Naik, B.; Rustagi, S. Biochar production methods and their transformative potential for environmental remediation. *Discov. Appl. Sci.* **2024**, *6*, 408. [CrossRef]
2. Guo, M.; Song, W.; Tian, J. Biochar-facilitated soil remediation: Mechanisms and efficacy variations. *Front. Environ. Sci.* **2020**, *8*, 521512. [CrossRef]
3. Al-Rubaye, H.A.; Yu, J.; Smith, J.D.; Al-Abedi, H.J. Experimental investigation of tar recycling in pilot-scale down-draft biomass gasifiers: Prospects, operating procedures, process variations, and controls. *Biofuels* **2023**, *14*, 201–210. [CrossRef]
4. Alfè, M.; Gargiulo, V.; Porto, M.; Migliaccio, R.; Le Pera, A.; Sellaro, M.; Pellegrino, C.; Abe, A.A.; Urciuolo, M.; Caputo, P.; et al. Pyrolysis and gasification of a real refuse-derived fuel (RDF): The potential use of the products under a circular economy vision. *Molecules* **2022**, *27*, 8114. [CrossRef] [PubMed]
5. Golpour, H.; Boravelli, T.; Smith, J.D.; Safarpour, H.R. Production of syngas from biomass using a downdraft gasifier. *Int. J. Eng. Res. Appl.* **2017**, *7*, 61–71. [CrossRef]
6. Sher, F.; Hameed, S.; Omerbegović, N.S.; Chupin, A.; Hai, I.U.; Wang, B.; Teoh, Y.H.; Yildiz, M.J. Cutting-edge biomass gasification technologies for renewable energy generation and achieving net zero emissions. *Energy Convers. Manag.* **2025**, *323*, 119213. [CrossRef]
7. Bhavanam, A.; Sastry, R. Biomass gasification processes in downdraft fixed bed reactors: A review. *Int. J. Chem. Eng. Appl.* **2011**, *2*, 425.
8. Fryda, L.; Visser, R. Biochar for soil improvement: Evaluation of biochar from gasification and slow pyrolysis. *Agriculture* **2015**, *5*, 1076–1115. [CrossRef]
9. Ulusal, A.; Varol, E.A.; Bruckman, V.J.; Uzun, B.B. Opportunity for sustainable biomass valorization to produce biochar for improving soil characteristics. *Biomass Convers. Biorefin.* **2021**, *11*, 1041–1051. [CrossRef]
10. Al-Abedi, H.J.; Smith, J.D.; Al-Rubaye, H.; Shakor, Z.M.; Erdem, A.; Ani, P.C. Synergistic co-pyrolysis of corn stover and refuse-derived fuel with microplastics: Kinetic and thermodynamic study. *Biofuels* **2024**, *15*, 1197–1213. [CrossRef]
11. Al-Abedi, H.J.; Smith, J.D.; Al-Rubaye, H.; Ani, P.C.; Moellenhoff, C.; McLeland, T.; Zagorac, K. Experimental and Aspen Simulation Study of the Co-Pyrolysis of Refuse-Derived Fuel and Oil Shale: Product Yields and Char Characterization. *Fuels* **2025**, *6*, 38. [CrossRef]
12. Rezaei, H.; Panah, F.Y.; Lim, C.J.; Sokhansanj, S. Pelletization of refuse-derived fuel with varying compositions of plastic, paper, organic, and wood. *Sustainability* **2020**, *12*, 4645. [CrossRef]
13. Zhao, L.; Giannis, A.; Lam, W.-Y.; Lin, S.-X.; Yin, K.; Yuan, G.-A.; Wang, J.-Y. Characterization of Singapore RDF resources and analysis of their heating value. *Sustain. Environ. Res.* **2016**, *26*, 51–54. [CrossRef]
14. Robinson, T.; Bronson, B.; Gogolek, P.; Mehrani, P. Air-blown bubbling fluidized bed co-gasification of woody biomass and refuse-derived fuel. *Can. J. Chem. Eng.* **2017**, *95*, 55–61. [CrossRef]
15. Abbas, S.; Abbas, A.; Zahra, T.; Kazmi, J.; Ahmad, W.; Ahmed, N.; Lim, T.M.; Cong, H. Green and gram-scale synthesis of uniform graphene quantum dots from biomass waste: A highly selective probe for nanomolar Hg^{2+} sensing. *Mater. Today Chem.* **2025**, *47*, 102830. [CrossRef]
16. Pattnaik, B.K.; Behera, R.; Santra, S.C.; Choudhury, S.; Biswas, J.K.; Hossain, A.; Moulick, D. Potentials of urban waste-derived biochar in minimizing heavy metal bioavailability: A techno-economic review. *Iscience* **2025**, *28*, 111915. [CrossRef]

17. Kumar, A.; Joseph, S.; Tsechansky, L.; Privat, K.; Schreiter, I.J.; Schüth, C.; Graber, E.R. Biochar aging in contaminated soil promotes Zn immobilization due to changes in biochar surface structural and chemical properties. *Sci. Total Environ.* **2018**, *626*, 953–961. [CrossRef]
18. Santos, D.C.B.D.; Evaristo, R.B.W.; Dutra, R.C.; Suarez, P.A.Z.; Silveira, E.A.; Ghesti, G.F. Advancing biochar applications: A review of production processes, analytical methods, decision criteria, and pathways for scalability and certification. *Sustainability* **2025**, *17*, 2685. [CrossRef]
19. Nworie, F.S.; Mgbemena, N.; Ike-Amadi, A.C.; Ebunoha, J. Functionalized biochars for enhanced removal of heavy metals from aqueous solutions: Mechanism and future industrial prospects. *J. Hum. Earth Future* **2022**, *3*, 377–395. [CrossRef]
20. Bachmann, H.J.; Bucheli, T.D.; Dieguez-Alonso, A.; Fabbri, D.; Knicker, H.; Schmidt, H.-P.; Ulbricht, A.; Becker, R.; Buscaroli, A.; Buerge, D.; et al. Toward the standardization of biochar analysis: The cost action TD1107 interlaboratory comparison. *J. Agric. Food Chem.* **2016**, *64*, 513–527. [CrossRef]
21. Li, S.; Tasnady, D. Biochar for soil carbon sequestration: Current knowledge, mechanisms, and future perspectives. *J. Carbon Res.* **2023**, *9*, 67. [CrossRef]
22. Verma, A.; Sharma, G.; Kumar, A.; Dhiman, P.; Stadler, F.J. Recent Advancements in Biochar and its Composite for the Remediation of Hazardous Pollutants. *Curr. Anal. Chem.* **2025**, *21*, 15–56. [CrossRef]
23. Vijayaraghavan, K. The importance of mineral ingredients in biochar production, properties and applications. *Crit. Rev. Environ. Sci. Technol.* **2021**, *51*, 113–139. [CrossRef]
24. Syguła, E.; Świechowski, K.; Stępień, P.; Koziel, J.A.; Białowiec, A. The prediction of calorific value of carbonized solid fuel produced from refuse-derived fuel in the low-temperature pyrolysis in CO_2. *Materials* **2020**, *14*, 49. [CrossRef]
25. Ani, P.C.; Alhameedi, H.; Al-Abedi, H.J.; Al-Rubaye, H.; Zeitoun, Z.; Ewuzie, U.; Smith, J.D. The Comprehensive Quantification and Characterization of Oak Biochar Produced via a Gasification Process Using a Downdraft Reactor. *Fuels* **2025**, *6*, 51. [CrossRef]
26. *ISO 18115-1*; Surface Chemical Analysis—Vocabulary—Part 1: General Terms and Terms Used in Spectroscopy. International Organization for Standardization: Geneva, Switzerland, 2013.
27. Kaszuba, M.; Corbett, J.; Watson, F.M.; Jones, A. High-concentration zeta potential measurements using light-scattering techniques. *Philos. Trans. R. Soc. A Math. Phys. Eng. Sci.* **2010**, *368*, 4439–4451. [CrossRef] [PubMed]
28. Makino, K.; Ohshima, H. Electrophoretic mobility of a colloidal particle with constant surface charge density. *Langmuir* **2010**, *26*, 18016–18019. [CrossRef] [PubMed]
29. Nzediegwu, C.; Naeth, M.A.; Chang, S.X. Elemental composition of biochars is affected by methods used for its determination. *J. Anal. Appl. Pyrolysis* **2021**, *156*, 105174. [CrossRef]
30. Lefebvre, J.; Galli, F.; Bianchi, C.L.; Patience, G.S.; Boffito, D.C. Experimental methods in chemical engineering: X-ray photoelectron spectroscopy-XPS. *Can. J. Chem. Eng.* **2019**, *97*, 2588–2593. [CrossRef]
31. Gale, M.; Nguyen, T.; Moreno, M.; Gilliard-AbdulAziz, K.L. Physiochemical properties of biochar and activated carbon from biomass residue: Influence of process conditions to adsorbent properties. *ACS Omega* **2021**, *6*, 10224–10233. [CrossRef]
32. Kabir, E.; Kim, K.-H.; Kwon, E.E. Biochar as a tool for the improvement of soil and environment. *Front. Environ. Sci.* **2023**, *11*, 1324533. [CrossRef]
33. Zhang, J.; Zhang, Y.; Zhao, W.; Li, Z.; Zang, L. Facile fabrication of calcium-doped carbon for efficient phosphorus adsorption. *ACS Omega* **2020**, *6*, 327–339. [CrossRef] [PubMed]
34. Hu, A.; Jiang, Y.; An, J.; Huang, X.; Elgarhy, A.H.; Cao, H.; Liu, G. Novel Fe/Ca oxide co-embedded coconut shell biochar for phosphorus recovery from agricultural return flows. *RSC Adv.* **2024**, *14*, 27204–27214. [CrossRef] [PubMed]
35. Liu, L.; Huang, L.; Huang, R.; Lin, H.; Wang, D. Immobilization of heavy metals in biochar derived from co-pyrolysis of sewage sludge and calcium sulfate. *J. Hazard. Mater.* **2021**, *403*, 123648. [CrossRef] [PubMed]
36. Peng, X.; Islam, S.; Li, Q.; Fu, Q.; Zhu, J.; Hu, H. Combined Application of Biochar and Calcium Superphosphate Can Effectively Immobilize Cadmium and Reduce Its Uptake by Cabbage. *Agronomy* **2024**, *14*, 2538. [CrossRef]
37. Zhao, L.; Cao, X.; Mašek, O.; Zimmerman, A. Heterogeneity of biochar properties as a function of feedstock sources and production temperatures. *J. Hazard. Mater.* **2013**, *256*, 1–9. [CrossRef]
38. Bahcivanji, L.; Gascó, G.; Paz-Ferreiro, J.; Méndez, A. The effect of post-pyrolysis treatment on waste biomass-derived hydrochar. *Waste Manag.* **2020**, *106*, 55–61. [CrossRef]
39. Liu, Z.; Quek, A.; Hoekman, S.K.; Balasubramanian, R. Production of solid biochar fuel from waste biomass by hydrothermal carbonization. *Fuel* **2013**, *103*, 943–949. [CrossRef]
40. Gao, P.; Hu, Z.; Sheng, Y.; Pan, W.; Ding, L.; Tang, L.; Chen, X.; Wang, F. Pyrolysis of municipal plastic waste: Chlorine distribution and formation of organic chlorinated compounds. *Sci. Total Environ.* **2024**, *912*, 169572. [CrossRef]
41. Strezov, V.; Zhou, X.; Evans, T.; Kan, T.; Taylor, M.P. Investigation of the effect of chlorine in different additives on dioxin formation during high temperature processing of iron ore. *Ecotoxicol. Environ. Saf.* **2024**, *288*, 117406. [CrossRef]
42. Yang, P.; Jia, D.; Lin, B.; Zhuang, X.; Bi, X. Microwave-assisted catalytic pyrolysis of refuse-derived fuel (RDF) to improve pyrolysis performance and biochar properties. *Fuel Process. Technol.* **2022**, *227*, 107129. [CrossRef]

43. Barman, R.; Gupta, A.; Kandpal, G. Combined Application of Biochar with Fertilizers Influence available Nitrogen, Phosphorus and Potassium Quantity in Soil. *Int. J. Curr. Microbiol. App. Sci.* **2019**, *8*, 1218–1224. [CrossRef]
44. Zou, X.; Debiagi, P.; Amjed, M.A.; Zhai, M.; Faravelli, T. Impact of high-temperature biomass pyrolysis on biochar formation and composition. *J. Anal. Appl. Pyrolysis* **2024**, *179*, 106463. [CrossRef]
45. Zeitoun, Z.; El-Shazly, A.H.; Nosier, S.; Elmarghany, M.R.; Salem, M.S.; Taha, M.M. Performance evaluation and kinetic analysis of photocatalytic membrane reactor in wastewater treatment. *Membranes* **2020**, *10*, 276. [CrossRef]
46. Michalak, I.; Baśladyńska, S.; Mokrzycki, J.; Rutkowski, P. Biochar from a freshwater macroalga as a potential biosorbent for wastewater treatment. *Water* **2019**, *11*, 1390. [CrossRef]
47. Moradi-Choghamarani, F.; Moosavi, A.A.; Baghernejad, M. Determining organo-chemical composition of sugarcane bagasse-derived biochar as a function of pyrolysis temperature using proximate and Fourier transform infrared analyses. *J. Therm. Anal. Calorim.* **2019**, *138*, 331–342. [CrossRef]
48. Liu, Y.; He, Z.; Uchimiya, M. Comparison of biochar formation from various agricultural by-products using FTIR spectroscopy. *Mod. Appl. Sci.* **2015**, *9*, 246. [CrossRef]
49. Li, B.; Huang, Y.; Wang, Z.; Li, J.; Liu, Z.; Fan, S. Enhanced adsorption capacity of tetracycline on tea waste biochar with $KHCO_3$ activation from aqueous solution. *Environ. Sci. Pollut. Res.* **2021**, *28*, 44140–44151. [CrossRef]
50. Ganesan, K.; Guin, B.; Wilbanks, E.; Sternberg, J. Synthesis and Characterization of Soy Hull Biochar-Based Flexible Polyurethane Foam Composites. *Materials* **2025**, *18*, 2006. [CrossRef]
51. Ben Salem, I.; El Gamal, M.; Sharma, M.; Hameedi, S.; Howari, F.M. Utilization of the UAE date palm leaf biochar in carbon dioxide capture and sequestration processes. *J. Environ. Manag.* **2021**, *299*, 113644. [CrossRef]
52. Hou, J.; Yu, J.; Li, W.; He, X.; Li, X. The effects of chemical oxidation and high-temperature reduction on surface functional groups and the adsorption performance of biochar for sulfamethoxazole adsorption. *Agronomy* **2022**, *12*, 510. [CrossRef]
53. Fan, Q.; Cui, L.; Quan, G.; Wang, S.; Sun, J.; Han, X.; Wang, J.; Yan, J. Effects of wet oxidation process on biochar surface in acid and alkaline soil environments. *Materials* **2018**, *11*, 2362. [CrossRef] [PubMed]
54. Beć, K.B.; Grabska, J.; Badzoka, J.; Huck, C.W. Spectra-structure correlations in NIR region of polymers from quantum chemical calculations. The cases of aromatic ring, C=O, C≡ N, and C-Cl functionalities. *Spectrochim. Acta Part A Mol. Biomol. Spectrosc.* **2021**, *262*, 120085. [CrossRef] [PubMed]
55. Tao, W.; Zhang, P.; Li, H.; Yang, Q.; Oleszczuk, P.; Pan, B. Generation mechanism of persistent free radicals in lignocellulose-derived biochar: Roles of reducible carbonyls. *Environ. Sci. Technol.* **2022**, *56*, 10638–10645. [CrossRef] [PubMed]
56. Yang, C.X.; Zhu, Q.; Dong, W.P.; Fan, Y.Q.; Wang, W.L. Preparation and characterization of phosphoric acid-modified biochar nanomaterials with highly efficient adsorption and photodegradation ability. *Langmuir* **2021**, *37*, 9253–9263. [CrossRef]
57. Wang, Z.; Li, J.; Zhang, G.; Zhi, Y.; Yang, D.; Lai, X.; Ren, T. Characterization of acid-aged biochar and its ammonium adsorption in an aqueous solution. *Materials* **2020**, *13*, 2270. [CrossRef]
58. Liu, A.; Feng, L.-J.; Ou, Y.; Zhang, X.; Zhang, J.; Chen, H. Competitive adsorption of polycyclic aromatic hydrocarbons on phosphorus tailing-modified sludge biochar provides mechanistic insights. *Environ. Geochem. Health* **2024**, *46*, 497. [CrossRef]
59. Reddy, P.M.K.; Krushnamurty, K.; Mahammadunnisa, S.K.; Dayamani, A.; Subrahmanyam, C. Preparation of activated carbons from bio-waste: Effect of surface functional groups on methylene blue adsorption. *Int. J. Environ. Sci. Technol.* **2015**, *12*, 1363–1372. [CrossRef]
60. Ramezanzadeh, H.; Zarehaghi, D.; Baybordi, A.; Bouket, A.C.; Oszako, T.; Alenezi, F.N.; Belbahri, L. The impacts of biochar-assisted factors on the hydrophysical characteristics of amended soils: A review. *Sustainability* **2023**, *15*, 8700. [CrossRef]
61. Enaime, G.; Baçaoui, A.; Yaacoubi, A.; Lübken, M. Biochar for wastewater treatment—Conversion technologies and applications. *Appl. Sci.* **2020**, *10*, 3492. [CrossRef]
62. Yu, P.; Baker, M.C.; Crump, A.R.; Vogler, M.; Strawn, D.G.; Möller, G. Biochar integrated reactive filtration of wastewater for P removal and recovery, micropollutant catalytic oxidation, and negative CO_2e: Process operation and mechanism. *Water Environ. Res.* **2023**, *95*, e10926. [CrossRef]
63. Zhou, J.; Yang, P.; Kots, P.A.; Cohen, M.; Chen, Y.; Quinn, C.M.; de Mello, M.D.; Boscoboinik, J.A.; Shaw, W.J.; Caratzoulas, S.; et al. Tuning the reactivity of carbon surfaces with oxygen-containing functional groups. *Nat. Commun.* **2023**, *14*, 2293. [CrossRef] [PubMed]
64. Dong, H.; Zhang, L.; Shao, L.; Wu, Z.; Zhan, P.; Zhou, X.; Chen, J. Versatile strategy for the preparation of woody biochar with oxygen-rich groups and enhanced porosity for highly efficient Cr (VI) removal. *ACS Omega* **2021**, *7*, 863–874. [CrossRef] [PubMed]
65. Hong, M.; Zhang, L.; Tan, Z.; Huang, Q. Effect mechanism of biochar's zeta potential on farmland soil's cadmium immobilization. *Environ. Sci. Pollut. Res.* **2019**, *26*, 19738–19748. [CrossRef] [PubMed]
66. Bayar, J.; Ali, N.; Dong, Y.; Ahmad, U.; Anjum, M.M.; Khan, G.R.; Zaib, M.; Jalal, A.; Ali, R.; Ali, L. Biochar-based adsorption for heavy metal removal in water: A sustainable and cost-effective approach. *Environ. Geochem. Health* **2024**, *46*, 428. [CrossRef]
67. Blanco-Canqui, H. Biochar and water quality. *J. Environ. Qual.* **2019**, *48*, 2–15. [CrossRef]

68. Boçe, M.T.; Hoxha, J. Blockchain technology as a catalyst for sustainable development: Exploring economic, social, and environmental synergies. *Acad. J. Interdiscip. Stud.* **2024**, *13*, 151. [CrossRef]
69. Chaves Fernandes, B.C.; Ferreira Mendes, K.; Dias Júnior, A.F.; da Silva Caldeira, V.P.; da Silva Teófilo, T.M.; Severo Silva, T.; Mendonça, V.; de Freitas Souza, M.; Valadão Silva, D. Impact of pyrolysis temperature on the properties of eucalyptus wood-derived biochar. *Materials* **2020**, *13*, 5841. [CrossRef]
70. Long, L.; Xue, Y.; Hu, X.; Zhu, Y. Study on the influence of surface potential on the nitrate adsorption capacity of metal modified biochar. *Environ. Sci. Pollut. Res.* **2019**, *26*, 3065–3074. [CrossRef]
71. Tomczyk, A.; Sokołowska, Z.; Boguta, P. Biochar physicochemical properties: Pyrolysis temperature and feedstock kind effects. *Rev. Environ. Sci. Bio/Technol.* **2020**, *19*, 191–215. [CrossRef]
72. Valentim, B.; Białecka, B.; Gonçalves, P.A.; Guedes, A.; Guimarães, R.; Cruceru, M.; Całus-Moszko, J.; Popescu, L.G.; Predeanu, G.; Santos, A.C. Undifferentiated inorganics in coal fly ash and bottom ash: Calcispheres, magnesiacalcispheres, and magnesiaspheres. *Minerals* **2018**, *8*, 140. [CrossRef]
73. Santos, A.C.; Cruz, C.; Font, E.; French, D.; Guedes, A.; Moreira, K.; Sant'ovaia, H.; Vieira, B.J.C.; Waerenborgh, J.C.; Valentim, B. Physicochemical properties of Fe-bearing phases from commercial Colombian coal ash. *Minerals* **2023**, *13*, 1055. [CrossRef]
74. Araujo, R.O.; Anjos, O.C.D.; Souza, L.K.D.; Bataglion, G.A. Biochar from Lignocellulosic Biomass: A Sustainable Circular Economy Approach For Removing Organic And Inorganic Contaminants. *Química Nova* **2024**, *47*, e-20240079. [CrossRef]
75. Pandian, K.; Vijayakumar, S.; Mustaffa, M.R.A.F.; Subramanian, P.; Chitraputhirapillai, S. Biochar—A sustainable soil conditioner for improving soil health, crop production and environment under changing climate: A review. *Front. Soil Sci.* **2024**, *4*, 1376159. [CrossRef]